Regularization parameter estimation for non-negative hyperspectral image deconvolution:supplementary material

Yingying Song, David Brie, El-Hadi Djermoune, Simon Henrot

Regularization parameter estimation for non-negative hyperspectral image deconvolution: supplementary material

Yingying Song, David Brie, El-Hadi Djermoune, Simon Henrot

This document is a supplementary material aiming at evaluating the performances of the proposed MDC and MCC for different types of hyperspectral images. Also, it gives an application of these approaches on real data.

I. Simulation examples

These simulations aim at investigating the behavior of the MDC and MCC for different types of hyperspectral images. In particular, we address the following questions:

- What are the performances of the 2 criteria?
- Does the estimated regularization parameters reflect the very nature (peaky or smooth) of the hyperspectral images to recover?
- Does the number of zeros in the hyperspectral images influence the performance of the criterion?

A. Simulated hyperspectral images

The simulation examples are generated according to the instantaneous mixture model

$$\mathbf{X} = \sum_k \mathbf{A}_k \circ \mathbf{s}_k \tag{1}$$

Here $\mathbf{A}_k$ represents the k-th abundance (spatial source) which is a function of the spatial variables, $\mathbf{s}_k$ represents the k-th endmember (spectral source) and $\circ$ is the outer (tensor) product.

Five different types of data are simulated.

TABLE I: Simulation examples

Data	$\mathbf{A}_k$	$\mathbf{s}_k$
Example 1	Peaky with many zeros	Smooth and positive
Example 2	Smooth with many zeros	Peaky with many zeros
Example 3	Smooth with less zeros	Peaky and positive
Example 4	Very Smooth and positive	Peaky with many zeros
Example 5	Very smooth and positive	Smooth and positive

The PSF (convolution filter) $\mathcal{H}_l$ is a low-pass gaussian filter of size (11×11) and its full width at half maximum is 5 points in both dimensions. The PSF is invariant with respect to l. The blurring is implemented in the Fourier domain (circular convolution).

B. Performance evaluation and result presentation

We used the fast implementation of MCC and MDC. For each example, the performance evaluation is conducted by estimating the mean square error (MSE) as a function of the signal-to-noise ratio (SNR). Each MSE value is obtained by averaging three trials corresponding to 3 random noise realizations. We also show the standard deviation of the estimated MSE. The images resulting from the deconvolution at SNR=20 dB are also presented.

C. Results

Example 1 is the one presented in the paper (see sections 5.B and 5.C). The results are not reported here.

This work has been supported by the FUI AAP 2015 Trispirabois Project and the Conseil Régional de Lorraine.

Centre de Recherche en Automatique de Nancy (CRAN), Université de Lorraine, CNRS, Boulevard des Aiguilletes B.P. 239 F-54506 Vandœuvre-lès-Nancy, France (email: firstname.lastname@univ-lorraine.fr for Yingying Song, David Brie and El-Hadi Djermoune; simon.henrot@gmail.com for Simon Henrot).

Example 2

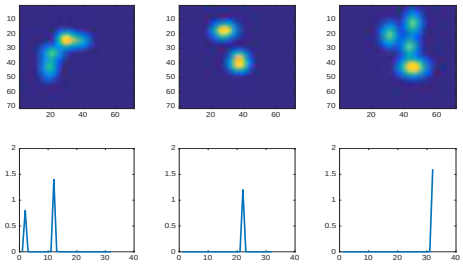

Fig. 1: Abundance maps and endmembers of example 2.

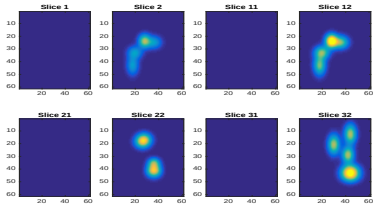

(a) Unblurred hyperspectral image

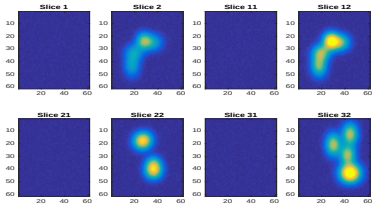

(b) Blurred noisy hyperspectral image $\mathbf{y}$ (SNR= 20 dB)

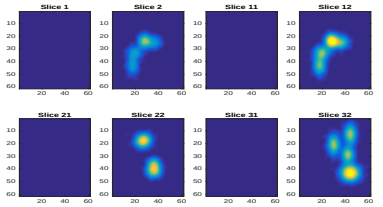

(c) Deconvolution with parameters found by the MCC ($\mu_s = 9.9370$, $\mu_\lambda = 0.0166$)

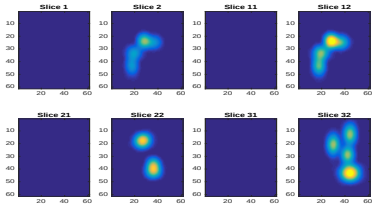

(d) Deconvolution with parameters found by the MDC ($\mu_s = 193.5059$, $\mu_\lambda = 0.0166$)

Fig. 2: Results of the non-negative deconvolution problem using MCC and MDC

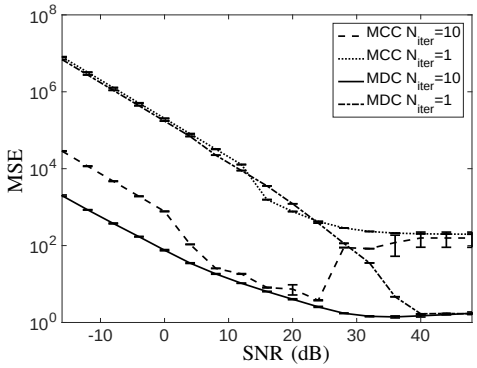

Fig. 3: Performances of the hyperspectral image deconvolution with optimal parameters (μ_s, μ_λ) selected by MCC and MDC

Example 3

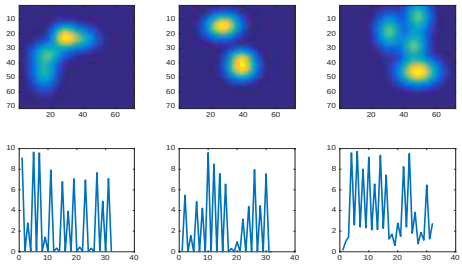

Fig. 4: Abundance maps and endmembers of example 3.

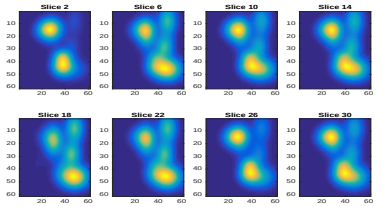

(a) Unblurred hyperspectral image

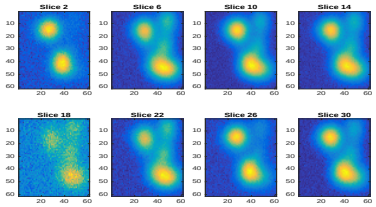

(b) Blurred noisy hyperspectral image $\mathbf{y}$ (SNR= 20 dB)

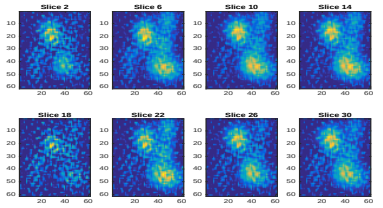

(c) Deconvolution with parameters found by the MCC ($\mu_s = 0.0131$, $\mu_\lambda = 854.8111$

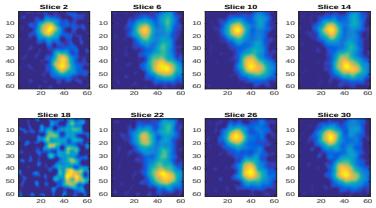

(d) Deconvolution with parameters found by the MDC ($\mu_s = 18.5917$, $\mu_\lambda = 0.1170$)

Fig. 5: Results of the non-negative deconvolution problem using MCC and MDC

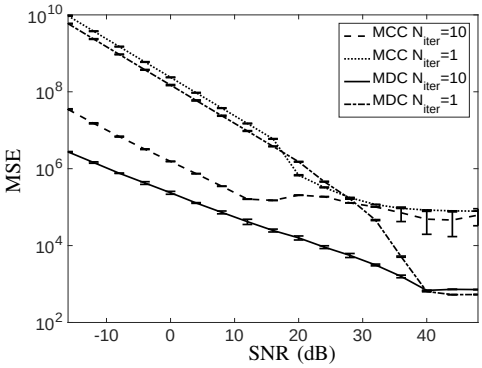

Fig. 6: Performances of the hyperspectral image deconvolution with optimal parameters (μ_s, μ_λ) selected by MCC and MDC

Example 4

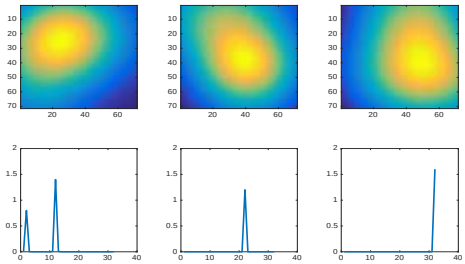

Fig. 7: Abundance maps and endmembers of example 4.

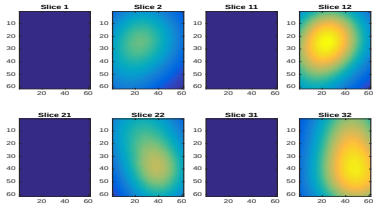

(a) Unblurred hyperspectral image

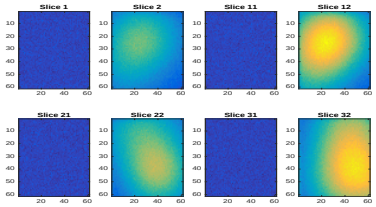

(b) Blurred noisy hyperspectral image $\mathbf{y}$ (SNR= 20 dB)

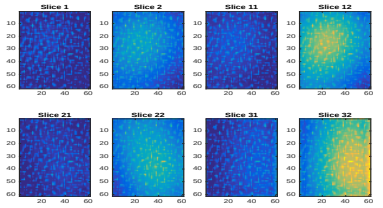

(c) Deconvolution with parameters found by the MCC ($\mu_s = 0.0113$, $\mu_\lambda = 735.9349$)

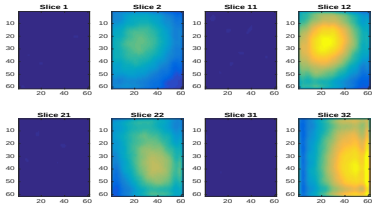

(d) Deconvolution with parameters found by the MDC ($\mu_s = 731.8141$, $\mu_\lambda = 1.3294$)

Fig. 8: Results of the non-negative deconvolution problem using MCC and MDC

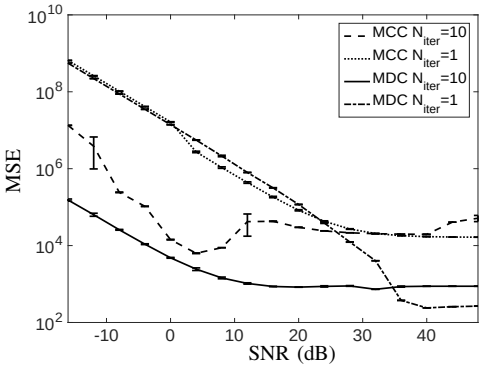

Fig. 9: Performances of the hyperspectral image deconvolution with optimal parameters (μ_s, μ_λ) selected by MCC and MDC

Example 5

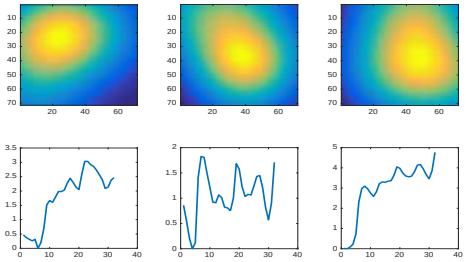

Fig. 10: Abundance maps and endmembers of example 5.

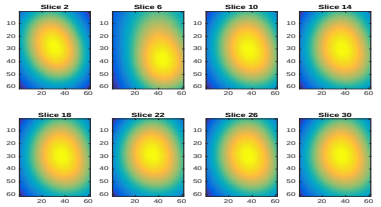

(a) Unblurred hyperspectral image

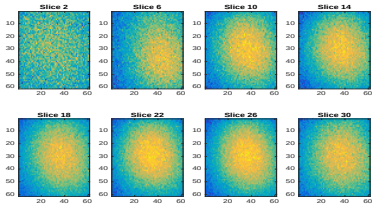

(b) Blurred noisy hyperspectral image $\mathbf{y}$ (SNR= 20 dB)

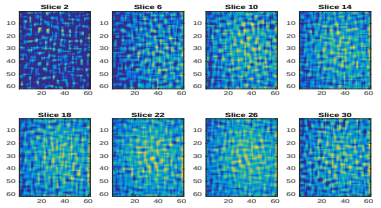

(c) Deconvolution with parameters found by the MCC ($\mu_s = 0.1498$, $\mu_\lambda = 3.2279$)

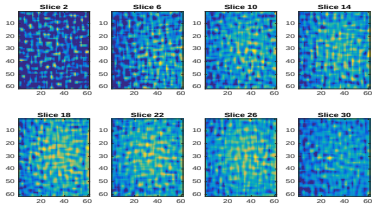

(d) Deconvolution with parameters found by the MDC ($\mu_s = 0.5575$, $\mu_\lambda = 0.8785$)

Fig. 11: Results of the non-negative deconvolution problem using MCC and MDC

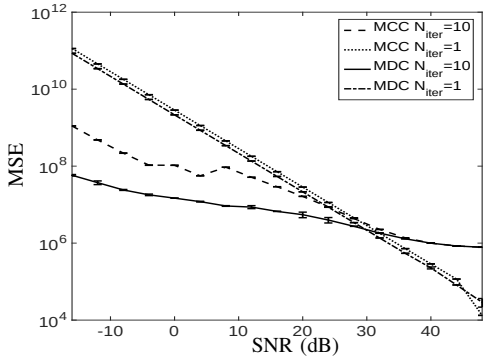

Fig. 12: Performances of the hyperspectral image deconvolution with optimal parameters (μ_s, μ_λ) selected by MCC and MDC

D. Discussion

The analysis of the results shows that MDC always performs better than MCC. Also, the corresponding MSEs are more stable (smooth) than those of MCC. This is due to the multiple maximum problem of MCC which renders the MSE behavior a bit erratic.

The non-negativity constraint really matters when the image includes many zeros. Increasing the number of points on which the positivity constraint is active, will also increase the folding of the response surface resulting in an accurate regularization parameter estimation. When the number of zeros is low, the non-negativity constraint is no longer relevant and the corresponding MDC and MCC are not very efficient. It may even happen that, for high SNR, the unconstrained deconvolution (associated MDC and MCC) yields better solutions. See in the supplementary material, example 5 (which is a kind of worst-case scenario) for SNR > 30 dB.

Finally, the estimated regularization parameters with MDC (associated to non-negative deconvolution) is linked to the nature of the image to recover. Spatially (resp. spectrally) smooth images yield large values of μ_s (resp. μ_λ). Conversely, spatially (resp. spectrally) peaky images yield low values of μ_s (resp. μ_λ). It corresponds to what intuition suggests. This is another evidence of the interest of MDC.

II. Real-world example

A. Data acquisition

The example provided here corresponds to an image of bacterial biosensors using hyperspectral fluorescence microscopy. A bacterial biosensor is a genetically modified bacteria which reacts to a stressing element (here iron, Fe) by producing a fluorescent protein (GFP). The hyperspectral fluorescence images will give indications of the Fe spatial concentration. This hyperspectral image is size is $(512 \times 512 \times 16)$ and the pixel size is $0.117\,\mu$m along each dimention. The 16 wavelengths are ranging from 455nm to 605nm. It was obtained by Carl Zeiss Bio-Rad confocal microscope. The PSF of the microscope is evaluated according to [1] as a function of the imaging parameters (excitation wavelength, emission wavelength, numerical aperture and pixel size). This results in a 7×7 Gaussian approximation of the PSF.

B. Results

Figure 13 shows the raw data (upper row), the restored data with the regularization parameters estimated by MCC (middle row) and the restored data with the regularization parameters estimated by MDC (lower row). Figure 14 and 15 are two parts selected from figure 13. It should be noted that this data cube includes both peaky and smooth parts along the spectral dimension; this makes the choice of a global spectral regularization parameter not obvious. A large regularization parameter will over-smooth the peaky part while a low regularization parameter will under-regularize the smooth part.

Both results show an improved resolution. However looking carefully at the results of MCC, reveals that the spectral regularization parameter is over estimated. This results in a spectral over-smoothing which makes some high intensity patterns of bacteria remaining on adjacent spectral bands (see for example Fig. 14(b)). This is less visible for MDC.

References

[1] B. Zhang, J. Zerubia, and J.-C. Olivo-Marin, "Gaussian approximations of fluorescence microscope point-spread function models," *Applied Optics*, vol. 46, no. 10, pp. 1819–1829, 2007.

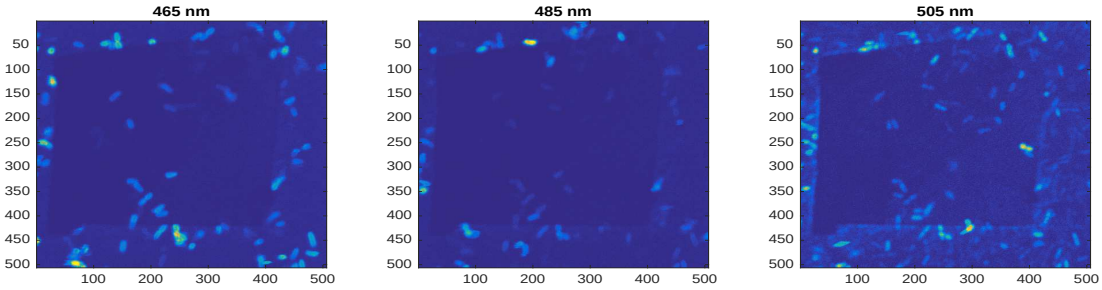

(a) Real hyperspectral image $\mathbf{y}$

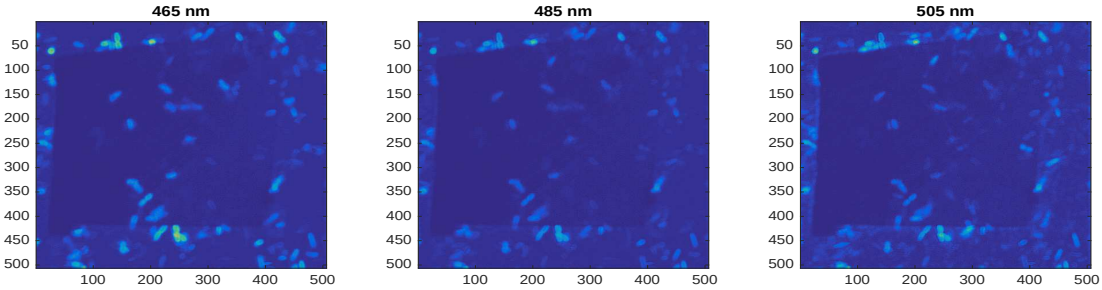

(b) MCC ($\mu_s = 0.0047$, $\mu_\lambda = 4.3528$

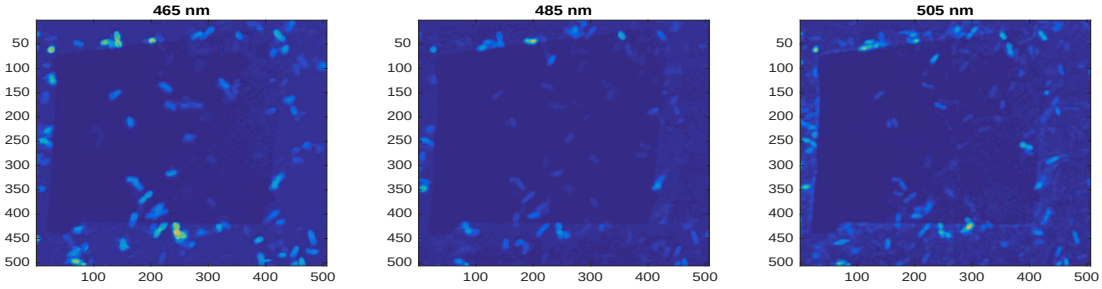

(c) MDC ($\mu_s = 0.2505$, $\mu_\lambda = 0.6115$)

Fig. 13: Results of the non-negative deconvolution problem using MCC and MDC

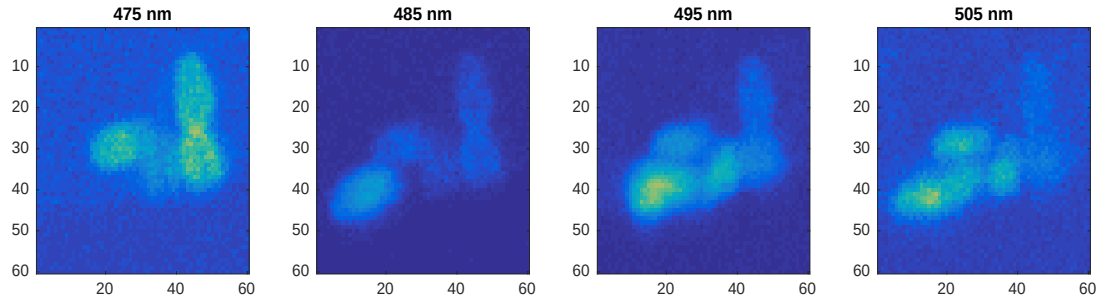

(a) Real hyperspectral image $\mathbf{y}$

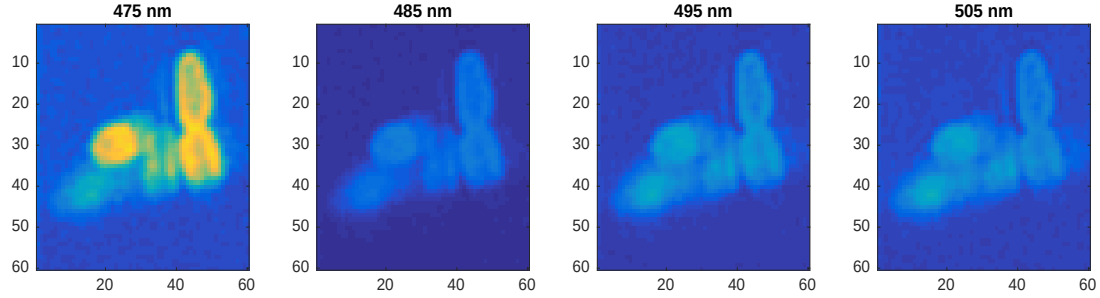

(b) MCC ($\mu_s = 0.0047$, $\mu_\lambda = 4.3528$)

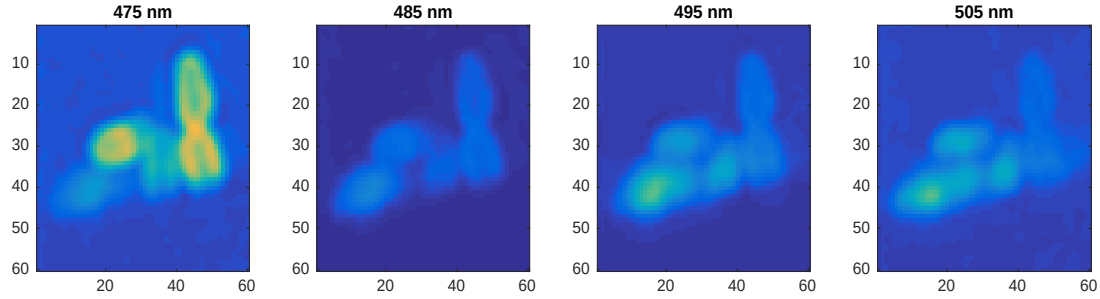

(c) MDC ($\mu_s = 0.2505$, $\mu_\lambda = 0.6115$)

Fig. 14: Results of the non-negative deconvolution problem using MCC and MDC

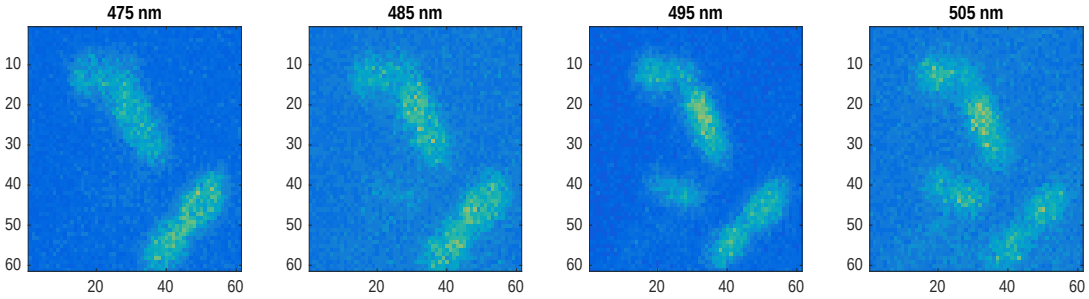

(a) Real hyperspectral image $\mathbf{y}$

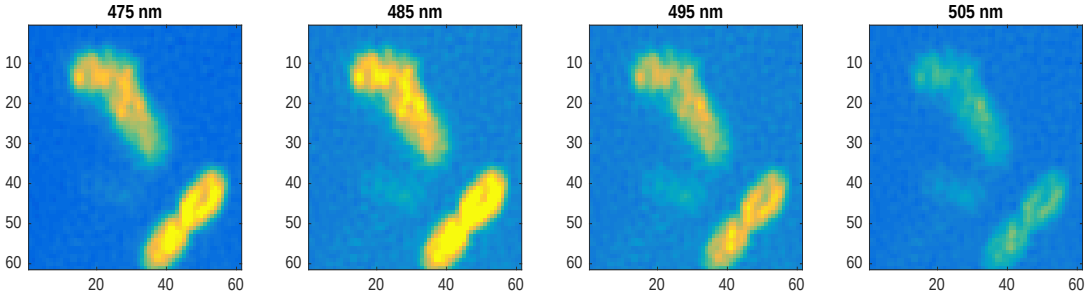

(b) MCC ($\mu_s = 0.0047$, $\mu_\lambda = 4.3528$)

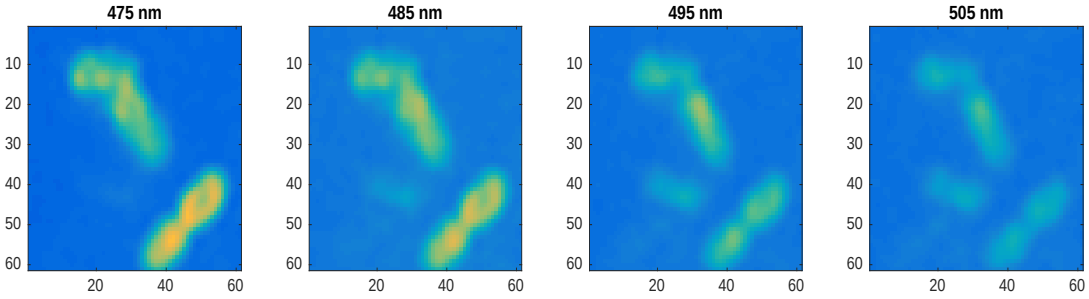

(c) MDC ($\mu_s = 0.2505$, $\mu_\lambda = 0.6115$)

Fig. 15: Results of the non-negative deconvolution problem using MCC and MDC